

Generative Multi-Agent Q-Learning for Policy Optimization: Decentralized Wireless Networks

Talha Bozkus and Urbashi Mitra

Abstract—*Q*-learning is a widely used reinforcement learning (RL) algorithm for optimizing wireless networks, but faces challenges with large state-spaces. Recently proposed multi-environment mixed *Q*-learning (MEMQ) algorithm addresses these challenges by employing multiple *Q*-learning algorithms across multiple synthetically generated, distinct but structurally related environments, so-called *digital cousins*. In this paper, we propose a novel multi-agent MEMQ (M-MEMQ) for *cooperative decentralized* wireless networks with multiple networked transmitters (TXs) and base stations (BSs). TXs do not have access to global information (joint state and actions). The new concept of *coordinated* and *uncoordinated* states is introduced. In *uncoordinated* states, TXs act independently to minimize their individual costs and update local *Q*-functions. In *coordinated* states, TXs use a Bayesian approach to estimate the joint state and update the joint *Q*-functions. The cost of information-sharing scales linearly with the number of TXs and is independent of the joint state-action space size. Several theoretical guarantees, including deterministic and probabilistic convergence, bounds on estimation error variance, and the probability of misdetecting the joint states, are given. Numerical simulations show that M-MEMQ outperforms several decentralized and centralized training with decentralized execution (CTDE) multi-agent RL algorithms by achieving 55% lower average policy error (APE), 35% faster convergence, 50% reduced runtime complexity, and 45% less sample complexity. Furthermore, M-MEMQ achieves comparable APE with significantly lower complexity than centralized methods. Simulations validate the theoretical analyses.

Index Terms—Multi-agent reinforcement learning, decentralized *Q*-learning, wireless networks, digital cousins.

I. INTRODUCTION

Reinforcement learning (RL) is a powerful framework for optimizing next-generation wireless networks that can be modeled as Markov Decision Processes (MDPs) [1], [2]. When the MDP dynamics, such as transition probabilities and cost functions, are unknown, model-free RL algorithms such as *Q*-learning can be employed. *Q*-learning is a simple, tabular, and model-free RL algorithm and works with discrete and modest-sized state-action spaces [3]. However, it faces several challenges, including slow convergence, high sample complexity, high estimation bias, and variance, and training instability across large state-action spaces [4], [5].

We have proposed multi-environment mixed *Q*-learning (MEMQ) to tackle these issues by running multiple *Q*-learning

algorithms across multiple, distinct yet structurally related synthetic environments – *digital cousins* and fusing their *Q*-functions into a single ensemble *Q*-function estimate using adaptive weighting [4]–[8]. MEMQ has three distinct features compared to the existing *Q*-learning algorithms. First, MEMQ constructs multiple, synthetic, distinct yet structurally related environments during training. These environments have been shown to help accelerate the exploration of the state-space [4]. Second, MEMQ trains multiple *Q*-learning agents on these environments and combines their outputs into an ensemble *Q*-function to achieve more robust *Q*-functions with lower variance [4]. Third, MEMQ uses a mixed-learning strategy – it combines real-time interactions with synthetic samples collected from the synthetic environments for faster training with improved sample complexity [4], [5].

MEMQ was originally designed for single-agent centralized MISO and MIMO wireless networks to solve real-world challenges such as resource allocation and interference minimization with lower complexity. However, it is not directly applicable to multi-agent and decentralized wireless networks. To this end, multi-agent RL (MARL) theory can be used to extend single-agent MEMQ to multi-agent networks. MARL has been effectively applied to different wireless network optimization problems, including resource and power allocation, channel access, beamforming, spectrum management, and multi-access edge computing [9]–[15], and can be categorized along several dimensions. Different training strategies depend on how agents are trained and execute their decisions and include fully centralized [4], [16], centralized training decentralized execution (CTDE) [17], [18], decentralized with networked agents (DNA) [19], [20] and fully decentralized [21], [22]. If agents have complete visibility of the global state, it is fully observable; otherwise partially observable [23]. Different communication strategies may vary in terms of which agents communicate, when and how to establish communication links, what information to share, and how to combine the received messages [24]. Different coordination strategies depend on whether agents collaborate to achieve a common goal and include fully cooperative [25], fully competitive [26], or mixed [27]. If agents share the same observation and action space and have a common reward function, then they are *homogeneous* [28]; otherwise *heterogeneous* [29]. Other categorizations include value-based vs. policy-based methods, tabular vs. deep neural network approaches, online vs. offline vs. hybrid methods, and methods for discrete vs. continuous state-action spaces.

In this work, we develop a multi-agent MEMQ (M-MEMQ) algorithm for wireless networks with multiple decentralized but networked agents (i.e. transmitters). The system comprises

Talha Bozkus and Urbashi Mitra are with the Ming Hsieh Department of Electrical and Computer Engineering, University of Southern California, Los Angeles, USA. Email: {bozkus, ubli}@usc.edu.

This work was funded by the following grants: NSF CCF-1817200, ARMY W911NF1910269, ARO W911NF2410094, DOE DE-SC0021417, Swedish Research Council 2018-04359, NSF CCF-2008927, NSF CCF-2200221, NSF RINGS-2148313, UCD/NSF CCF-2311653, NSF A22-2666-S003, ONR 503400-78050, ONR N00014-15-1-2550, ONR N00014-22-1-2363, UCSD/NSF KR 705319, UCD/NSF A25-0139-S009.

multiple mobile transmitters (agents) and stationary base stations. The overall state-space is divided into *coordinated* and *uncoordinated* states. In uncoordinated states, agents operate under partial observability in a decentralized manner without access to global information (e.g., other agents' states, actions, or costs) and independently update their local Q -tables. In coordinated states, agents can locally measure the aggregated received signal strength (ARSS) due to other transmitters to estimate the joint state using maximum a posteriori probability (MAP) estimation and communicate with the leader agent by sharing limited information (i.e., their local Q -functions and costs) to cooperatively minimize the joint cost. Agents are homogeneous and share the same state-action spaces and cost functions. M-MEMQ inherits key characteristics of MEMQ – it is a value-based, off-policy algorithm and adopts a mixed-learning strategy. It is also a tabular algorithm and thus is applicable to moderately large discrete state-action spaces.

MARL face challenges such as partial observability, scalability, effective exploration and security concerns, non-stationary, and credit assignment [30]. Our proposed M-MEMQ algorithm can alleviate these challenges effectively. For example, while global information is not available to agents, they use MAP estimation based on their local observations to estimate the joint state. On the other hand, M-MEMQ offers a good balance between policy accuracy, runtime complexity, and communication costs across an increasing number of agents and larger state-action space, making it scalable. M-MEMQ also accelerates the exploration of the joint state-space by combining real-time interactions with synthetic samples collected from synthetic environments in real-time. The problem of non-stationary is alleviated through the leader agent, which uses a centralized Q -function update by aggregating information from individual agents to maintain a global system view. Finally, the leader agent updates the global Q -functions and determines the joint state and action, considering each agent's confidence in their joint state estimates, which prioritizes more confident agents by assigning them greater weight (i.e., credit) for their contributions.

Our approach herein is a form of *generative learning*, but differs from traditional generative methods such as generative adversarial networks [31]–[33]. We construct synthetic environments – synthetic simulators that RL agents can continuously interact with to generate synthetic training data alongside real data during training. Our approach is computationally efficient to implement, interpretable, and has strong theoretical guarantees. The synthetically generated data herein follow different, but related distribution to the real-time data and are augmented with real-time data to accelerate exploration [4], [5]. We observe that due to our exemplar application, wireless communication networks, our distinct agents actually experience different environments and dynamics in contrast to many MARL works [9]–[11].

The **main contributions** of this paper are as follows: (i) We develop the first multi-agent MEMQ algorithm (M-MEMQ) for decentralized wireless networks with networked agents. (ii) In coordinated states, agents estimate the joint state using a Bayesian MAP estimation based on local observations in a decentralized way to minimize the cost of information ex-

change. In the uncoordinated states, agents act independently. (iii) We provide the first theoretical guarantees for multi-agent MEMQ algorithms, including deterministic and probabilistic convergence, bounds on estimation error variance, and the probability of misdetecting the joint states. (iv) We evaluate our algorithm on a wireless network with multiple mobile transmitters (TX) and stationary base stations (BS) to find the optimal TX-BS association to minimize the joint wireless cost. Our algorithm outperforms several decentralized and CTDE-based MARL algorithms by achieving 55% lower average policy error (APE), 35% faster convergence rate, 50% less computational runtime complexity and %45 less sample complexity. Our algorithm achieves comparable APE with significantly lower complexity than centralized methods. In addition, our algorithm exhibits high robustness to changes in network parameters. Simulations verify theoretical analyses.

We use the following notation: the vectors are bold lower case (\mathbf{x}), matrices and tensors are bold upper case (\mathbf{A}), and sets are in calligraphic font (\mathcal{S}).

II. SYSTEM MODEL AND TOOLS

A. Markov Decision Processes

A **single agent MDP** is characterized by a 4-tuple $\{\mathcal{S}_i, \mathcal{A}_i, p_i, c_i\}$, where \mathcal{S}_i and \mathcal{A}_i denote the state and action spaces of agent i . The state and action of agent i at time t are $s_{i,t}$ and $a_{i,t}$, respectively. The transition probability from $s_{i,t}$ to $s'_{i,t}$ under action $a_{i,t}$ is $p_{a_{i,t}}(s_{i,t}, s'_{i,t})$, which is stored in the probability transition tensor (PTT) \mathbf{P}_i , and the incurred cost is $c_i(s_{i,t}, a_{i,t})$. The agent i aims to solve the following infinite-horizon discounted cost minimization equation (*Bellman's optimality*) [3]:

$$v_i^*(s_i) = \min_{\pi_i} v_{\pi_i}(s_i) = \min_{\pi_i} \mathbb{E}_{\pi_i} \sum_{t=0}^{\infty} \gamma^t c_i(s_{i,t}, a_{i,t}), \quad (1)$$

where v_{π_i} is the value function (VF) under policy π_i , v_i^* is the optimal VF of agent i , and $\gamma \in (0, 1)$ is the discount factor.

A **multi-agent MDP** generalizes a single-agent MDP to N agents ($i = 1, 2, \dots, N$), each with its own states and actions. The joint state at time t is $\bar{s}_t = (s_{1,t}, \dots, s_{N,t})$ and the joint action is $\bar{a}_t = (a_{1,t}, \dots, a_{N,t})$. The joint state and action spaces are obtained as $\mathcal{S} = \otimes_{i=1}^N \mathcal{S}_i$ and $\mathcal{A} = \otimes_{i=1}^N \mathcal{A}_i$, where \otimes is the Kronecker product. The transition from joint state \bar{s}_t to \bar{s}'_t under joint action \bar{a}_t occurs with probability $p(\bar{s}_t, \bar{a}_t, \bar{s}'_t)$, which is stored in the joint probability transition tensor \mathbf{P} , and incurs joint cost $c_i(\bar{s}_t, \bar{a}_t)$ for agent i . The optimization problem of the multi (joint) agent is as follows:

$$\bar{v}^*(\bar{s}) = \min_{\bar{\pi}} \bar{v}_{\bar{\pi}}(\bar{s}) = \min_{\bar{\pi}} \mathbb{E}_{\bar{\pi}} \sum_{t=0}^{\infty} \gamma^t \sum_{i=1}^N c_i(\bar{s}_t, \bar{a}_t), \quad (2)$$

where $\bar{v}_{\bar{\pi}}$ is the joint value function under the joint policy $\bar{\pi}$ and \bar{v}^* is the optimal joint value function. If agents are independent (i.e. no interactions), the joint PTT \mathbf{P} is given by $\mathbf{P} = \otimes_{i=1}^N \mathbf{P}_i$; otherwise, \mathbf{P} accounts for agent interactions.

B. Q-Learning

When the system dynamics (transition probabilities and cost functions) are unknown or non-observable, Q -learning can be used to solve (1) and (2). **Single-agent Q-learning** solves (1) by learning the Q -functions of agent i , $Q_i(s_i, a_i)$, using the following update rule [3]:

$$Q_i(s_i, a_i) \leftarrow (1-\alpha)Q_i(s_i, a_i) + \alpha(c_i(s_i, a_i) + \gamma \min_{a'_i \in \mathcal{A}_i} Q_i(s'_i, a'_i)), \quad (3)$$

where $\alpha \in (0, 1)$ is the learning rate. Different exploration strategies, such as ϵ -greedy, softmax-exploration, or upper-confidence bound action selection, can be used to handle the exploration-exploitation trade-off to ensure sufficient sampling of different state-action pairs [3]. The agent interacts with the environment and collects samples $\{s_i, a_i, s'_i, c_i\}$ to update Q -functions using (3). Q -functions converge to their optimal values with probability one, given certain conditions [34]. The optimal policy is $\pi_i^*(s_i) = \operatorname{argmin}_{a_i \in \mathcal{A}_i} Q_i^*(s_i, a_i)$, and the relationship between the optimal value function and optimal Q -functions is $v_i^*(s_i) = \min_{a_i \in \mathcal{A}_i} Q_i^*(s_i, a_i)$. Q -learning is an **off-policy** algorithm because it optimizes a target policy (the optimal policy being learned) while using a different policy, such as ϵ -greedy, for exploration and interaction with the environment. In addition, Q -learning effectively works with small to moderately large discrete state-action spaces.

Different MARL training strategies can be employed to extend single-agent Q -learning to multiple agents to solve (2) depending on the availability of global information, observability of the joint state, or agents' ability to interact/communicate. The optimal joint policy and value functions can be obtained as $\bar{\pi}^*(\bar{s}) = \operatorname{argmin}_{\bar{a} \in \mathcal{A}} \bar{Q}^*(\bar{s}, \bar{a})$, and $\bar{v}^*(\bar{s}) = \min_{\bar{a} \in \mathcal{A}} \bar{Q}^*(\bar{s}, \bar{a})$ where \bar{Q}^* is the optimal joint Q -functions. The sizes of the Q -tables for Q_i and \bar{Q} are $|\mathcal{S}_i| \times |\mathcal{A}_i|$ and $|\mathcal{S}| \times |\mathcal{A}|$, respectively. In this work, all agents are assumed to share the same state-action space size (i.e., $|\mathcal{S}_i| \times |\mathcal{A}_i|$ is the same for all i).

C. Single-agent Multi-environment Mixed Q-Learning

MEMQ algorithm leverages the novel concept of *digital cousins* proposed in [4], [5]. Digital cousins are multiple synthetically created, structurally related but distinct environments. Let i subscript denote agent i . In MEMQ, the agent i interacts with K_i environments simultaneously: one real environment (Env_1), and $K_i - 1$ synthetic environments (Env_n), where each Env_n ($n > 1$) represents a unique digital cousin of the real environment. For example, the agent interacts with two environments in Fig.2b: one real ('REAL') and one synthetic ('SYNTHETIC'), where the order n is generic and not shown).

We herein briefly review the work of [4]. The agent i first estimates the PTT of the real environment in real-time by sampling. Let $\hat{\mathbf{P}}_i$ denote the estimated PTT. Simultaneously, it constructs the PTT of synthetic environments as powers of $\hat{\mathbf{P}}_i$, with $\hat{\mathbf{P}}_i^n$ representing the estimated PTT of the n -th synthetic environment ¹. The agent runs K_i independent Q -learning algorithms across these environments, generating Q -functions

$Q_i^{(n)}$ for each Env_n . These Q -functions are combined into an ensemble Q -function, Q_i^e , using the update rule:

$$Q_i^e(s_i, a_i) = uQ_i^e(s_i, a_i) + (1-u) \sum_{n=1}^{K_i} w_i^{(n)} Q_i^{(n)}(s_i, a_i), \quad (4)$$

where the weights of environments $w_i^{(n)}$ is determined using some adaptive weighting mechanism, and u is the update ratio parameter [4]. It has been shown that Q_i^e converges to the optimal Q -functions in mean-square (i.e. $Q_i^e \xrightarrow{m.s.} Q^*$ for all i) faster than the individual Q -functions $Q_i^{(n)}$ given a particular structure on update ratio u [4].

Herein, K_i and n are hyperparameters. While K_i is chosen proportional to the state-action space size, selecting n is more challenging. For $K_i = 4$, there are many possible sets of orders (1,2,3,4 vs 1,2,3,5 vs 2,3,6,7 or similar). The goal is to use the fewest synthetic environments that provide the most diverse multi-time-scale information. To this end, we employ the coverage-coefficient environment selection algorithm that we developed for the single-agent case [35], [36], which selects the synthetic environments based on their sample coverage of the real environment.

We use the notations Q -function and Q -table interchangeably. For instance, $Q_i^{(n)}$ represents a generic Q -function for Env_n as well as the Q -table that stores Q -functions for Env_n . Meanwhile, $Q_i^{(n)}(s_i, a_i)$ refers to the Q -function for a specific state-action pair.

III. DECENTRALIZED WIRELESS NETWORK WITH MULTIPLE NETWORKED AGENTS

While our approach is general and has wide applications [4], [5], to make our approach and analysis more accessible, we first describe a decentralized wireless network framework with multiple agents, serving as a representative example of real-world network complexities and challenges.

We consider a grid environment of size $L \times L$ with cells of size $\Delta_L \times \Delta_L$. There are N_T mobile transmitters (TXs) and N_B stationary base stations (BSs), where each TX can move randomly in four directions (U, R, D, L) or stay stationary, all with equal probability. TXs always remain on grid points. Each BS_j has a circular coverage area with radius r_j ; a TX can connect to BS only on or within this area. Fig.1 shows an example wireless network with 3 TXs and 2 BSs, where red squares are BSs, green triangles are TXs, black solid circles show coverage areas, purple solid arrows represent a particular TX-BS association, black dotted arrows represent the communications between TXs, and TX_1 is assumed to be the leader TX that controls the coordination among agents (i.e. TXs communicate with **only** TX_1 when necessary). Herein, the leader TX is defined as the transmitter with the largest coverage area (radius r_j), as it can communicate with and broadcast to the largest portion of the network, ensuring better connectivity to base stations and other TXs. We underline that many hierarchical sensor and wireless networks have leader transmitters or nodes [37]. Each TX can continuously measure (sense) the aggregated received signal strength (ARSS) due to all other TXs. This is practical, as most wireless devices can easily obtain ARSS measurements, unlike CSI information,

¹There are alternative ways to construct the PTT of synthetic environments such as employing graph symmetrization methods [5].

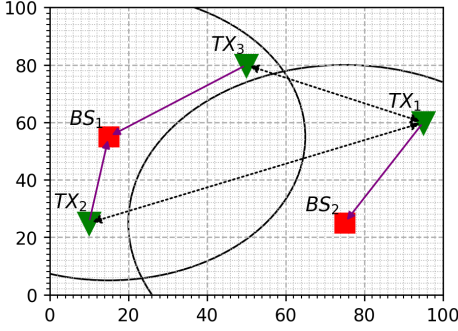


Fig. 1: Example wireless network setting

which requires specialized hardware [38]. We now describe the RL framework for the given wireless network.

1) *Agent*: TXs are the decision-making agents; hence, there are N_T agents. While TXs operate in a decentralized manner as the joint state information is not available (see next section), they are networked and can coordinate through the leader TX when coordination is necessary (see Section IV).

2) *State*: The individual state of TX $_i$ is a triplet $s_i = (x_i, y_i, I_i)$, where (x_i, y_i) is its location with $x_i, y_i \in [0, \Delta_L, 2\Delta_L, \dots, L]$, and I_i is the ARSS. Since ARSS may be continuous, we quantize I_i to the nearest value in $[I_{\min}, I_{\max}]$, which is discretized into equal steps of size Δ_I . The transition from (x_i, y_i) to (x'_i, y'_i) depends on the random movement of TX $_i$, while the transition from I_i to I'_i is influenced by several factors such as the random movement of all TXs, the distances between TXs, L , and I_{thr} . The joint state \bar{s} is the concatenation of individual states as $\bar{s} = (s_1, s_2, \dots, s_{N_T})$, and is **not** available to the agents (i.e. agents do not have access to each others' states).

The state-space is divided into two parts: *coordinated* and *uncoordinated* states. The joint state \bar{s} is *coordinated* if there is at least one strong ARSS measurement in the wireless network, i.e., there is at least one agent i such that $I_i > I_{thr}$, where I_{thr} is the predefined ARSS threshold; otherwise, it is *uncoordinated*. Thus, if at least one TX identifies the state as coordinated, it informs TX $_1$, which then broadcasts this information to all TXs. We denote $|\mathcal{S}_C|$ and $|\mathcal{S}_U|$ as the number of coordinated and uncoordinated states, which depend on I_{thr} , and $|\mathcal{S}_C| + |\mathcal{S}_U| = |\mathcal{S}|$.

We note that there are alternative approaches to determining coordinated states, such as based on predefined states [12], proximity between agents [39], and statistical analysis of prior trajectories [40]. Our approach is similar to [41], which also uses local RSS measurements to determine coordinated states. However, in our work, coordination is based on sufficiently high ARSS values. In addition, coordination is possible even if not all agents measure high ARSS levels. This makes our scheme robust against ARSS measurement inaccuracies in some agents, and scalable by reducing dependency on each agent's measurement.

3) *Action*: The action set of TX $_i$ is $\mathcal{A}_i = \{1, 2, \dots, N_B\}$, where each index corresponds to a specific BS that the TX may connect. If a TX is outside a BS's coverage area, the action is invalid and assigned an infinite cost to prevent selection.

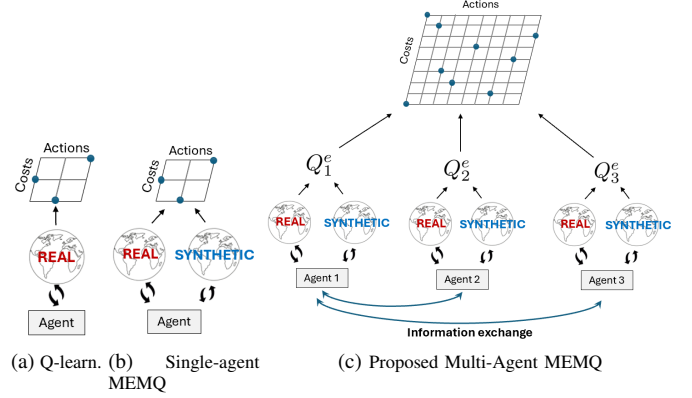


Fig. 2: Comparison of different Q-learning algorithms

Thus, $|\mathcal{A}_i| \leq N_B$. The joint action \bar{a} is the concatenation of individual actions as $\bar{a} = (a_1, a_2, \dots, a_{N_T})$, and $|\mathcal{A}| \leq N_B^{N_T}$.

4) *Cost function*: The individual cost function of TX $_i$ is as follows:

$$c_i = \beta_1 \frac{P_i}{\log_2(1 + \text{SNR}_i)} + \beta_2 Q(\sqrt{\text{SNR}_i}) + \beta_3 Q\left(\frac{I_{thr} - I_i}{\sigma}\right), \quad (5)$$

where $\text{SNR}_i = \frac{P_i}{d_i^2(n + I_i)}$, d_i is distance between TX $_i$ and the BS it is connected to, P_i is the transmission power of TX $_i$, and n is the zero-mean Gaussian noise as $n \sim \mathcal{N}(0, \sigma^2)$. Herein, the first component is the *efficiency cost*. A higher SNR with constant transmitting power improves the effective data rate and reduces the efficiency cost. The second component is the *reliability cost*. The Q -function represents the inverse relationship between SNR and bit error rate. Thus, higher SNR reduces the bit error rate and improves transmission reliability. The third component is the *fairness cost*. If the measured local ARSS exceeds the threshold I_{thr} , it suggests that some TXs are close to each other and may compete for the same resources (time slots, frequencies), potentially overloading some BSs while underutilizing others, which increases the fairness cost. The constants $\beta_1, \beta_2, \beta_3$ are the cost weights such that $\beta_1 + \beta_2 + \beta_3 = 1$. The joint cost is the sum of individual costs: $\bar{c} = \sum_{i=1}^{N_T} c_i(\bar{s}_i, \bar{a}_i)$. We emphasize that the individual cost function of each TX in (5) relies solely on local ARSS observations and does not depend on the knowledge of other TXs.

This cost function has several key properties. It is non-negative and bounded. It is highly non-linear and non-monotonic in some parameters (e.g., P_i), but monotonic in others (e.g., SNR and I_{thr}). Its non-convexity (due to the Gaussian Q -function) presents optimization challenges. The effect of different costs and parameters can be controlled through the weights β_i .

IV. ALGORITHM

A. Preliminaries and initialization

We describe our algorithm (Algorithm 1) using a three-agent wireless network ($N_T = 3$) to explain key details. However, our approach works for an arbitrary number of agents, as the wireless network setting in the previous section is described

Algorithm 1 Multi-Agent MEMQ (M-MEMQ)

Inputs: $l, \gamma, \alpha_t, \epsilon_t, u_t, \mathbf{b}_{i,0}, Q_i^{(n)}, Q_i^e$, wireless parameters
Outputs: $\bar{Q}, \bar{\pi}$

- 1: **for** $t = 1$ to T **do**
- 2: **for** each TX $_i$ **simultaneously do**
- 3: Reinitialize $\mathbf{b}_{i,t}$ if $\text{mod}(t, l) = 0$
- 4: Interact with Env $_1$, collect samples $\{s_i, a_i, s'_i, c_i\}$, and store in buffer \mathcal{B}_i
- 5: Sample $\{s_i, a_i, s'_i, c_i\}$ randomly from \mathcal{B}_i to update \mathbf{P}_i and the PTT of synthetic environment
- 6: Run MEMQ with real and synthetic environments
- 7: Determine if current state is coordinated based on local ARSS, and if so, estimate it using the Bayesian approach
- 8: Update the Q -functions as in Table II
- 9: **end for**
- 10: **end for**
- 11: $\bar{\pi}(\bar{s}) \leftarrow \text{argmin}_{\bar{a}'} \bar{Q}(\bar{s}, \bar{a}')$

for arbitrary N_T . Our simulations will explicitly consider larger values of N_T . Fig.2 illustrates the high-level comparison between standard Q -learning [3], single-agent MEMQ [4], and the proposed multi-agent MEMQ, where blue arrows show the direction of information exchange between agents and leader agent.

The inputs to Algorithm 1 are *algorithm parameters* (trajectory length l , discount factor γ , learning rate α_t , exploration probability ϵ_t , update ratio u_t , initial belief vectors $\mathbf{b}_{i,0}$ for agent i at $t = 0$, number of iterations T) and *wireless network parameters* ($L, \Delta_L, N_T, N_B, r_j, I_{min}, I_{max}, \Delta_I, \beta_1, \beta_2, \beta_3, P_i, k, I_{thr}, \sigma$). The outputs are the joint Q -table, \bar{Q} , and the corresponding joint policy, $\bar{\pi}$.

Each TX interacts with 2 environments as shown in Fig.2: the real environment (Env $_1$) and a single synthetic environment. The order of the synthetic environments for three TXs is chosen to be 2, 3, and 5, respectively, which are determined using the coverage-coefficient environment selection algorithm as explained in Sec.II-C. Hence, each TX keeps three different **local** Q -functions (i.e. Q -tables) as shown in Table I: two individual and one ensemble Q -functions. The leader TX, TX $_1$, also stores the joint Q -table \bar{Q} , which is updated based on the local Q -functions of all agents. We emphasize that $K = 2$ (i.e. one real and one synthetic environment for each agent) yields optimal performance for the given wireless network, yet our approach is compatible with any K ; other wireless networks such as in [5], [42] may require a larger K (and consequently different synthetic environments).

At the beginning of the algorithm, transmitters and base stations are also located randomly within the grid, while ensuring no collisions and sufficient distance between BSs.

B. Creating synthetic environments

Each TX $_i$ independently interacts with the real environment Env $_1$, collects samples $\{s_i, a_i, s'_i, c_i\}$, and stores this data in their buffer \mathcal{B}_i . Then, each TX $_i$ randomly samples from \mathcal{B}_i to update their individual estimated PTT for Env $_1$ ($\hat{\mathbf{P}}_i$), and simultaneously builds and updates the PTT of its synthetic environment ($\hat{\mathbf{P}}_i^n$) by taking the matrix power of $\hat{\mathbf{P}}_i$ as explained in Sec.II-C. We emphasize that creating synthetic environments is not a one-time process; the PTTs of synthetic environments are **continuously** updated as each TX continues

	Local Q -tables		Joint Q -table
	Individual	Ensemble	
TX $_1$	$Q_1^{(1)}, Q_1^{(2)}$	Q_1^e	\bar{Q}
TX $_2$	$Q_2^{(1)}, Q_2^{(3)}$	Q_2^e	-
TX $_3$	$Q_3^{(1)}, Q_3^{(5)}$	Q_3^e	-

TABLE I: Local and joint Q -tables in Algorithm 1

sampling from the real environment. Thus, the accuracy of the estimated synthetic environments improves over time.

We also reset belief updates and reinitialize belief vectors every l step to mitigate error accumulation from potentially erroneous initial belief vectors, noisy Q -functions, incorrect Q -function updates, or numerical errors during matrix power operations and improve adaptation to new observations. This section of the algorithm is given between lines 3 and 5.

C. Running MEMQ algorithms

While each TX $_i$ continuously updates its estimates for the PTT of real and synthetic environments, it also simultaneously runs a single-agent MEMQ algorithm using its two environments and continuously updates its local ensemble Q -functions Q_i^e . In other words, MEMQ algorithms are run on environments whose PTTs are continuously updated. This section of the algorithm is given in line 6.

The inputs to Algorithm 1 serve as inputs for the MEMQ algorithm of each TX. For example, P_i varies across different MEMQs, but I_{min} remains constant. While most inputs remain constant across different MEMQs, the different underlying PTTs and inherent randomness in sampling and exploration may lead to different convergence rates. As a result, this step of the algorithm is dominated by the slowest MEMQ.

We propose different single-agent MEMQ algorithms in our prior work [4]–[8]. While these algorithms share similar objectives and algorithm design, they have different assumptions and constraints on the underlying MDP and network parameters. We adopt the algorithm in [4] as it has the broadest applicability with minimal constraints and assumptions. For different wireless networks with specific assumptions or constraints, one may also employ the algorithms of [5]–[8].

D. Joint state estimation

While TXs can act independently in uncoordinated states, they need to coordinate in coordinated states to minimize the joint cost and update the joint Q -table. However, each TX has access to only local knowledge – they can continuously measure ARSS due to other TXs without further access to their individual states, actions, or costs. To this end, agents can estimate the joint state based on their local ARSS observations, and share limited information to obtain the joint action and costs. This approach, while not always optimal, ensures some level of privacy and significantly reduces information exchange cost [24].

In particular, agents use a Bayesian approach, akin to standard MAP estimation, to estimate the joint state in coordinated states based on their local ARSS observations. For TX $_1$, this involves estimating the joint state of TX $_2$ and TX $_3$ using the

State transition	Update rules
U → U	$Q_i^{(n)}(s_i, a_i) \leftarrow \text{Q-learning}, \quad Q_i^e(s_i, a_i) \leftarrow \text{MEMQ}, \quad \bar{Q}(\bar{s}, \bar{a}) = \sum_{i=1}^{N_T} Q_i^e(s_i, a_i).$
U → C	$Q_i^{(n)}(s_i, a_i) \leftarrow (1 - \alpha)Q_i^{(n)}(s_i, a_i) + \alpha[c_i(s_i, a_i) + \frac{\gamma}{3} \max_{\bar{a}'} \bar{Q}(\bar{s}', \bar{a}')], \quad Q_i^e(s_i, a_i) \leftarrow \text{MEMQ}$
C → U	$\bar{Q}(\bar{s}, \bar{a}) \leftarrow (1 - \alpha)\bar{Q}(\bar{s}, \bar{a}) + \alpha \sum_{i=1}^3 [c_i(\bar{s}, \bar{a}) + \gamma \max_{a_i'} Q_i^e(s_i', a_i')]$
C → C	$\bar{Q}(\bar{s}, \bar{a}) \leftarrow (1 - \alpha)\bar{Q}(\bar{s}, \bar{a}) + \alpha[\sum_{i=1}^3 c_i(\bar{s}, \bar{a}) + \gamma \max_{\bar{a}'} \bar{Q}(\bar{s}', \bar{a}')]$

TABLE II: Q-function update rules for different cases (time index subscript t is dropped for simplicity)

local ARSS measurement $I_{1,t}$ at time t . Let (s_2, s_3) be the actual states of TX₂ and TX₃ at time t , and (\hat{s}_2, \hat{s}_3) their estimates by TX₁. Then,

$$\hat{s}_2, \hat{s}_3 = \operatorname{argmax}_{s_2, s_3} p(s_2, s_3 | I_{1,t}), \quad (6)$$

$$= \operatorname{argmax}_{s_2, s_3} p(I_{1,t} | s_2, s_3) \mathbf{b}_{1,t}(s_2, s_3), \quad (7)$$

where the conditional distribution $p(I_{1,t} | s_2, s_3)$ follows a multivariate Normal distribution with mean vector $\boldsymbol{\mu}_{1,t}$ and covariance matrix $\boldsymbol{\Sigma}_{1,t}$, and $\mathbf{b}_{1,t}$ denotes TX₁'s belief vector at time t – the probability that TX₁ believes TX₂ and TX₃ are in states s_2 and s_3 , respectively. Herein, the parameters $\boldsymbol{\mu}_{1,t}$ and $\boldsymbol{\Sigma}_{1,t}$ depend on the ARSS measurements up to time t .

Then, the estimated joint state of the system by TX₁ is given by: $(s_1, \hat{s}_2, \hat{s}_3)$. Furthermore, the belief probabilities for the states (s_2, s_3) is updated as:

$$\mathbf{b}_{1,t+1}(s_2, s_3) \leftarrow p(I_{1,t} | s_2, s_3) \mathbf{b}_{1,t}(s_2, s_3), \quad (8)$$

$$\mathbf{b}_{1,t+1}(s_2, s_3) \leftarrow \operatorname{softmax}(\mathbf{b}_{1,t+1}(s_2, s_3)). \quad (9)$$

The joint state estimation for other TXs is done in a similar way; hence, each TX _{i} at time t has its own joint state estimate and a corresponding belief vector. The accuracy of joint state estimates varies among TXs depending on the quality of ARSS measurements, mean and covariance parameters, and initial belief vectors. This section of the algorithm is given in line 7.

Remark 1. We emphasize that the argmax operation in (7) is not an exhaustive discrete search over the entire state-space. The search at time t is restricted to a small subset of the state-space $\{s_{2,t} : \|s_{2,0} - s_{2,t}\|_2 \leq \Delta\} \times \{s_{3,t} : \|s_{3,0} - s_{3,t}\|_2 \leq \Delta\}$, where $\Delta = \delta_0 + 2\Delta_L \min(l, \operatorname{mod}(t, l))$ and the distance between the first estimated and true state is at most δ_0 [43]. Thus, the search space size is independent of the joint state-space size. We will numerically show that estimated states converge to the true states for modest values of Δ . A small δ_0 can be determined by analyzing the historical behavior of TXs, or leveraging domain knowledge. Without such knowledge, smaller trajectory lengths l or smaller grid size Δ_L also helps.

Remark 2. If the belief vector in (8) has also a multivariate Gaussian form as $\mathbf{b}_{1,t} \sim N(\boldsymbol{\mu}'_{1,t}, \boldsymbol{\Sigma}'_{1,t})$, then the uncertainty in the updated belief vector $\mathbf{b}_{1,t+1}$ monotonically decreases over time, i.e., $\boldsymbol{\Sigma}'_{1,t+1} \leq \boldsymbol{\Sigma}'_{1,t}$. This result can be shown using the properties of multivariate Gaussian. On the other hand, the updated mean depends on the local ARSS measurements, which vary over time as TXs move and channel conditions change, and hence may not change monotonically over time.

E. Local and joint Q-function updates

In Algorithm 1, the update of different Q-functions, as given in Table I depends on the transition direction between coordinated (C) and uncoordinated (U) states, as summarized in Table II. Individual Q-functions ($Q_i^{(n)}$ and Q_i^e) are updated in uncoordinated states, while the joint Q-function (\bar{Q}) is updated in coordinated states. In uncoordinated states, the joint Q-function is the sum of individual Q-functions since the TXs act independently.

In the coordinated states, TXs employ the following communication protocol: First, each TX independently estimates the joint state based on their local ARSS observations (as explained in Sec. IV-D) and shares the corresponding belief probability with the leader TX₁. Next, TX₁ selects the joint state with the highest belief probability and broadcasts the corresponding joint action. Each TX then executes its individual action and reports its costs and Q-functions to TX₁, which subsequently updates the joint Q-function. This section of the algorithm is given in line 8.

Remark 3. The cost of information exchange over T iterations among N_T agents is proportional to $O(N_T \max\{T, |\mathcal{S}_i| |\mathcal{A}_i|\})$, where O is the Big O notation, and i is a generic TX. [43]

This result shows that the cost of information exchange scales linearly with the number of agents as the leader TX coordinates and simplifies the coordination among agents. Additionally, the cost depends only on the individual state-action space size, rather than the joint state-action space size. These two factors allow for accommodating more agents without a significant increase in communication costs.

V. THEORETICAL ANALYSIS

We here provide several theoretical results for Algorithm 1.

A. Probabilistic Analysis

We first provide several probabilistic results. Our results are valid under the zero-mean distributional assumption on the Q-function errors of the n^{th} environment for all agents:

$$Q_{t,i}^{(n)}(s_i, a_i) - Q_i^*(s_i, a_i) \sim D_{i,n} \left(0, \frac{\lambda_{i,n}^2}{3} \right), \quad (10)$$

where $Q_{t,i}^{(n)}$ is the Q-function of n^{th} environment for agent i at time t , Q_i^* is the optimal Q-function of agent i , $D_{i,n}$ is some zero-mean distribution with estimation error variance $\frac{\lambda_{i,n}^2}{3}$.

This assumption is widely employed in RL literature: (i) it is used for non-MEMQ algorithms with $D_{i,n}$ being uniform

or normal for $n = 1$ case in [16], [44]; (ii) it is generalized to $n > 1$ with no assumptions on $D_{i,n}$ for MEMQ algorithms in [4]–[6], [43]; and (iii) it is employed in MEMQ algorithms with $D_{i,n}$ being uniform in [36]. These assumptions are also theoretically and numerically **justified** in [4]–[6], [43]. This assumption is generalized to multiple agents in this work. We emphasize that this assumption is used solely to facilitate our theoretical analysis and may not hold exactly in practice. However, the assumption can be relaxed by allowing $D_{i,n}$ to have a non-zero mean while constraining a weighted sum of means to equal zero, which may be more feasible in practice [4]. Our theoretical results **hold** under both cases.

We herein leverage probabilistic results in [4], which were derived for the single-agent MEMQ to derive our results for multi-agent MEMQ. Hence, the proof techniques in [4] can be adapted here to prove these results. These results hold for any number of agents (N_T) and number of environments (K_i).

Proposition 1. Let \bar{s} be an uncoordinated joint state. Then, the following holds for all t :

$$\mathbb{V}\left(\bar{Q}_t(\bar{s}, \bar{a}) - \sum_{i=1}^{N_T} Q_i^*(s_i, a_i)\right) \leq \sum_{i=1}^{N_T} \frac{f_i(\lambda_i)}{K_i}, \quad (11)$$

where $\lambda_i = \max_n \lambda_{i,n}$ is the estimation error variance of the worst environment for agent i , and f_i is some function of the parameter λ_i .

This proposition has several implications. First, as the number of environments (K_i) increases, the upper bound on the estimation error variance decreases, which is consistent with the variance-reduction property of ensemble RL algorithms. Second, even if some agents employ a small number of environments, the estimation error variance can still be reduced by employing a larger number of environments for other agents, which differs from the single-agent case [4], where employing a smaller number of environments always lead to a larger estimation variance. Third, the function f_i can be fine-tuned to further reduce the upper bound (see [4]). Finally, this result gives us the behavior of the estimation error variance in the finite t case. Hence, the variance reduction property of Algorithm 1 holds even for small t when the algorithm may be significantly far from convergence.

Corollary 1. The upper bound in (11) can also be expressed as a function of the update ratio u asymptotically in time as:

$$\lim_{t \rightarrow \infty} \mathbb{V}\left(\bar{Q}_t(\bar{s}, \bar{a}) - \sum_{i=1}^{N_T} Q_i^*(s_i, a_i)\right) \leq \frac{1-u}{1+u} \sum_{i=1}^{N_T} \lambda_i. \quad (12)$$

This result indicates that even with a large number of agents (N_T), the estimation error variance can be reduced by choosing a large u or using a time-varying u_t (such that $u_t \xrightarrow{t \rightarrow \infty} 1$) as in [4]. In practice, one can either optimize K_i (from Proposition 1) or u , depending on which parameter is easier to adjust. While optimizing K_i offers more control as there are N_T parameters to adjust, finding the optimal set may be challenging. In contrast, optimizing u provides less control but is more straightforward as it is the same for all agents. Similar to optimizing K_i in Proposition 1, even if some agents

have large λ_i and are computationally difficult to optimize, the upper bound can still be controlled by optimizing the worst environments of other agents, unlike the single-agent case [4].

Corollary 2. Let \bar{s} be an uncoordinated joint state. Then, the joint Q -functions converge to the sum of the optimal individual Q -functions of all agents in mean square:

$$\lim_{t \rightarrow \infty} \bar{Q}_t(\bar{s}, \bar{a}) \xrightarrow{\text{in mean square}} \sum_{i=1}^{N_T} Q_i^*(s_i, a_i). \quad (13)$$

This result demonstrates that, in uncoordinated states, the optimal joint Q -functions can be obtained by summing the individual Q -functions of all agents. This result relates Q -tables of different sizes (\bar{Q} : $|\mathcal{S}| \times |\mathcal{A}|$ vs \bar{Q}_i : $|\mathcal{S}_i| \times |\mathcal{A}_i|$) unlike [4], which considers Q -tables of the same size.

B. Deterministic Analysis

We now provide several deterministic results. These results are valid without any assumptions on Q -functions such as (10). We adapt the deterministic results and techniques from [5], which were originally derived for single-agent MEMQ, to establish our results herein for multi-agent MEMQ.

Proposition 2. Let \bar{s} be an uncoordinated joint state. Let the joint Q -function update at time t be $\bar{\Delta}_t(\bar{s}, \bar{a}) = \bar{Q}_t(\bar{s}, \bar{a}) - \bar{Q}_{t-1}(\bar{s}, \bar{a})$. Then, the following holds:

$$\lim_{t \rightarrow \infty} |\bar{\Delta}_t(\bar{s}, \bar{a}) - \bar{\Delta}_{t-1}(\bar{s}, \bar{a})| = 0. \quad (14)$$

This proposition provides insight into the behavior of the joint Q -function updates over time. As more iterations are performed, the updates to the joint Q -function become increasingly stable, indicating the stabilization of the overall learning process. This result applies to joint Q -functions and thus provides generalization over to the single-agent case [5], which is restricted to individual Q -functions. We leverage the stability of each MEMQ agent from [5] to derive the stability of the joint system. The proof is given in Appendix A.

Corollary 3. Let \bar{s} be an uncoordinated joint state. Then, it requires at most t_β iterations to ensure that $|\bar{\Delta}_t(\bar{s}, \bar{a})| \leq \beta$ for any $\beta > 0$, where:

$$t = \frac{\log\left(1 - \frac{\beta}{\sum_{i=1}^{N_T} \sum_{n=1}^{K_i} \theta_i^{(n)}(s_i, a_i)}\right)}{\log(u)}, \quad (15)$$

and u is the constant update ratio, $\theta_i^{(n)}(s_i, a_i)$ is the smallest constant satisfying $|\epsilon_{i,t}^{(n)}(s_i, a_i)| \leq \theta_i^{(n)}(s_i, a_i)$ for all t , and $\epsilon_{i,t}^{(n)}(s_i, a_i) = w_{i,t}^{(n)} Q_{i,t}^{(n)}(s_i, a_i) - w_{i,t-1}^{(n)} Q_{i,t-1}^{(n)}(s_i, a_i)$ is the weighted Q -function update of n^{th} environment for agent i .

This result is valid for any t ; thus, it can be used as a stopping condition for Algorithm 1. Moreover, by appropriately choosing the parameters u and K_i , we can effectively control the speed of convergence and the accuracy of the Q -function updates. This result reflects the sample complexity of Algorithm 1 to achieve β -convergence – this result is different than the standard sample complexity, which considers $\bar{Q}_t - \bar{Q}^*$ yet we herein consider $\bar{Q}_t - \bar{Q}_{t-1}$. This result considers

the aggregated performance of all agents and requires more iterations to match the sample complexity of the single-agent case [4].

Proposition 3. Let \bar{s} be an uncoordinated joint state. If $|\epsilon_{i,t-1}^{(n)}(s_i, a_i)| \leq |\epsilon_{i,t}^{(n)}(s_i, a_i)|$ for all n, t, i , then:

$$\lim_{t \rightarrow \infty} |\bar{\Delta}_t(\bar{s}, \bar{a})| = 0. \quad (16)$$

This proposition provides a sufficient deterministic condition for the convergence of Algorithm 1 in uncoordinated states. Unlike Corollary 2, which assumes zero-mean errors in Q -functions, this result only requires the monotonicity of the weighted Q -function updates.

C. Analysis of State Misdetection Probability

In real-world wireless networks, RSS measurements are noisy due to several factors, including interference from nearby transmitters, multipath propagation, or environmental factors such as physical obstacles [38]. To this end, we employ the noisy ARSS measurement model as follows:

$$I_{i,t} = I_{i,t,\text{true}} + n_t, \quad (17)$$

where $I_{i,t}$ and $I_{i,t,\text{true}}$ are the noisy and true ARSS measurement by TX_i due to the other transmitters at time t and n_t is additive zero-mean Gaussian noise as: $n_t \sim N(0, \sigma_u^2)$ in uncoordinated states and $n_t \sim N(0, \sigma_c^2)$ in coordinated states. In uncoordinated states, transmitters are often far apart from each other, leading to higher measurement uncertainty due to a lack of information exchange. Conversely, in coordinated states, closer proximity and synchronization reduce this uncertainty. Hence, we assume $\sigma_u \gg \sigma_c$.

Proposition 4. Assume there are $N_T = 2$ transmitters, and $|\mathcal{S}_C|\sigma_u > |\mathcal{S}_U|\sigma_c$. Under the noisy ARSS model (17), the probability of misdetecting the state as coordinated or uncoordinated is bounded as:

$$P_{\text{mis}} \in \left[Q\left(\frac{\Delta_I}{\sigma_c}\right) \frac{|\mathcal{S}_C|}{|\mathcal{S}|} + Q\left(\frac{-\Delta_I}{\sigma_u}\right) \frac{|\mathcal{S}_U|}{|\mathcal{S}|}, \right. \\ \left. Q\left(\frac{-\Delta_I}{\sigma_c}\right) \frac{|\mathcal{S}_C|}{|\mathcal{S}|} + Q\left(\frac{\Delta_I}{\sigma_u}\right) \frac{|\mathcal{S}_U|}{|\mathcal{S}|} \right], \quad (18)$$

where $Q(z) = \frac{1}{2} \text{erfc}\left(\frac{z}{\sqrt{2}}\right)$, and erfc is the complementary error function, and

$$\Delta_I = \sqrt{2 \ln \left(\frac{|\mathcal{S}_C|\sigma_u}{|\mathcal{S}_U|\sigma_c} \right) \left(\frac{1}{\sigma_c^2} - \frac{1}{\sigma_u^2} \right)^{-1}}. \quad (19)$$

The lower bound represents the fundamental limit on detection accuracy due to noise in ARSS measurements, reflecting an unavoidable misdetection error. The upper bound indicates the maximum misdetection probability, representing the worst-case scenario where the system is most vulnerable to errors from noisy ARSS measurements. We note that the lower and upper bounds are complementary and sum to 1. Thus, an increase in the lower bound directly results in a decrease in upper bound, and vice versa. For example, as σ_c increases, the lower bound increases, indicating a higher minimum error

probability. On the other hand, the upper bound decreases because higher noise in coordinated states causes the ARSS measurements to resemble those of uncoordinated states. As a result, the likelihood of misdetecting all states in the worst-case scenario decreases. When $|\mathcal{S}_C| \rightarrow |\mathcal{S}_U|$ and $\sigma_C \rightarrow \sigma_U$, both bounds converge to 0.5, indicating that the system can no longer distinguish between coordinated and uncoordinated states, leading to random detection. The proof is given in Appendix B.

Corollary 4. The bounds on the probability of misdetection can be generalized to any number of agents $N_T > 2$ using Taylor series approximation as follows: (See [45] for proof)

$$P_{\text{mis}} \in \left[\left(1 - \sum_{i=1}^{N_T} Q\left(\frac{I_{\text{thr}}^* - I_{i,t,\text{true}}}{\sigma_c}\right) \right) \frac{|\mathcal{S}_C|}{|\mathcal{S}|} + \right. \\ \left. Q\left(\frac{I_{\text{thr}}^* - I_{i',t,\text{true}}}{\sigma_u}\right) \frac{|\mathcal{S}_U|}{|\mathcal{S}|}, \right. \\ \left. \sum_{i=1}^{N_T} Q\left(\frac{I_{\text{thr}}^{**} - I_{i,t,\text{true}}}{\sigma_u}\right) \frac{|\mathcal{S}_U|}{|\mathcal{S}|} + \right. \\ \left. \left(1 - Q\left(\frac{I_{\text{thr}}^{**} - I_{i',t,\text{true}}}{\sigma_c}\right) \right) \frac{|\mathcal{S}_C|}{|\mathcal{S}|} \right], \quad (20)$$

where I_{thr}^* and I_{thr}^{**} are two distinct constants as a (non-linear) function of N_T , $|\mathcal{S}_C|$, $|\mathcal{S}_U|$, σ_c , σ_u and the minimum true ARSS measurement among all agents $I_{i',t,\text{true}} = \min_{i=1,\dots,N_T} I_{i,t,\text{true}}$.

This result is derived using a second-order Taylor series approximation of the Gaussian $Q(x)$ function around $x = 0$ and hence is numerically accurate when the threshold I_{thr} is close to the true ARSS measurements $I_{i,t,\text{true}}$ or when noise variances σ_c and σ_u are large. It is possible to employ a higher-order Taylor approximation for a more precise bound, yet it becomes harder to derive a closed-form expression. The lower and upper bounds herein are complementary (i.e., one increases while the other one decreases) as in the two-agent case. We will numerically analyze the effect of individual parameters on the tightness of the bound.

Proposition 4 and Corollary 4 present novel results compared to the single-agent case [4], [5]. These results are derived for the wireless network in Sec.III using the ARSS model (17); however, similar results can be derived for the multi-agent versions of MISO and MIMO networks in [5] with different ARSS models such as multiplicative noise model e.g. $I_{i,t} = h_t I_{i,t,\text{true}} + n_t$, with h_t being the fading coefficient or interference noise model $I_{i,t} = I_{i,t,\text{true}} + \sum_{j \neq i} I_{j,t,\text{interference}} + n_t$.

VI. NUMERICAL RESULTS

In this section, we consider a variety of performance metrics to assess the accuracy and complexity performance of Algorithm 1. The following parameters are constant across all simulations: $T = 10^5$, $l = 30$, $\gamma = 0.95$, $\alpha_t = \frac{1}{1+t/1000}$, $\epsilon_t = \max(0.99^t, 0.01)$, $u_t = 1 - e^{-t/1000}$ (if constant $u = 0.5$), $L = 100$, $\Delta_L = 2$, $r_j \sim \text{unif}\left[\frac{L}{2}, \frac{3L}{4}\right]$, $\Delta_I = 50$, $\sigma = 1$, $P_i = 10^{-2}$, $\beta_1 = \beta_2 = \beta_3 = \frac{1}{3}$. The parameters I_{max} and I_{min} are set to the max and min ARSS measurements for each simulation. The parameters $\lambda_{i,n}$ are estimated numerically

Algorithm	Type
Randomized Ensembled Double Q-learning (REDQ) [16]	Fully centralized
Multi-agent Deep Q-Networks (DQN) [17]	CTDE
QD-Learning (QD) [19]	DNA
Two-layer Q-learning (TQ) [20]	DNA
Ideal Independent Q-learning (I2Q) [22]	Fully decentralized
Hysteretic Q-learning (HQ) [21]	Fully decentralized

TABLE III: Different cooperative MARL algorithms

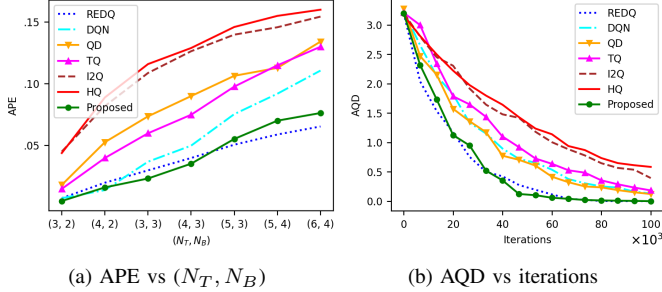


Fig. 3: Performance of different MARL algorithms

as in [4]. I_{thr} is chosen to be the minimizer of P_{mis} from Proposition 4 and Corollary 4. $|\mathcal{S}_c|$ and $|\mathcal{S}_u|$ are determined using I_{thr} . K_i is selected proportional to the state-space size as in [4], and remain constant for all i . The values of σ_c and σ_u are chosen such that $\sigma_u \gg \sigma_c$ and the assumption in Proposition 1 is satisfied. Parameters of joint state-estimation μ , Σ , δ_0 and $\mathbf{b}_{i,0}$ are determined as in [43]. Simulations are averaged over 100 independent simulations.

A. Policy and Q-function accuracy

We first define the *average policy error (APE)* as:

$$APE = \frac{1}{|\mathcal{S}|} \sum_{\bar{s}=1}^{|\mathcal{S}|} \mathbf{1}(\bar{\pi}^*(\bar{s}) \neq \bar{\pi}(\bar{s})) \quad (21)$$

where $\bar{\pi}^*$ is the optimal joint output policy from (2), and $\bar{\pi}$ is the joint output policy of Algorithm 1. We also define the *average Q-function distance (AQD)* as:

$$AQD = \frac{1}{|\mathcal{S}||\mathcal{A}|} \sum_{\bar{s}, \bar{a}} (\bar{Q}^*(\bar{s}, \bar{a}) - \bar{Q}(\bar{s}, \bar{a}))^2 \quad (22)$$

where \bar{Q}^* is the optimal joint Q-functions, and \bar{Q} is the joint output Q-functions of Algorithm 1 at time t . We evaluate our algorithm against several fully cooperative tabular and deep MARL algorithms as shown in Table III. These algorithms can be used with our wireless network setting and are chosen such that different MARL algorithms with different characteristics are represented.

APE results across an increasing number of transmitters and base stations (N_T, N_B) are shown in Fig.3a. Our algorithm offers 35% less APE than CTDE, 45% less APE than DNA, and 55% less APE than fully decentralized algorithms, particularly across large (N_T, N_B) . These APE gains can be attributed to the following reasons: (i) exchanging local ARSS information through the leader can effectively capture coordination among agents. (ii) Leveraging synthetic environments through MEMQ helps agents improve their exploration capabilities [4]. (iii)

Parameter	Range	Δ_{APE}	Δ_{AQD}
L	{40, 60, ... 400}	5%	6%
Δ_L	{1, 2, ... 10}	6%	10%
r_j	$\text{unif}[x, 3x], x \in \{\frac{L}{5}, \frac{L}{4}, \frac{L}{3}, \frac{L}{2}\}$	8%	8%
Δ_I	{10, 20, ... 100}	8%	12%
σ	{0.2, 0.4, ... 2}	6%	10%
P_i	$\{10^{-4}, 10^{-3}, 10^{-2}, 10^{-1}, 1\}$	6%	6%

TABLE IV: Impact of wireless parameters in performance.

MEMQ exploits structural similarities among multiple environments, providing an advantage over neural network-based algorithms that do not utilize such properties. (iv) Optimizing I_{thr} , by minimizing the state misdetection probability, achieves the optimal $|\mathcal{S}_c|/|\mathcal{S}_u|$ ratio, which combines coordination benefits in coordinated states and complexity gains in uncoordinated states. The centralized algorithm achieves slightly better APE than our algorithm, as expected since it assumes full observability among agents. However, the performance difference is minimal (only less than 10%) because (i) communication and information exchange among agents only in coordinated states are sufficient to capture coordination, and (ii) periodically resetting the belief state prevents error accumulation and yields accurate joint state estimates. We also note that APE improvements increase as the wireless network grows, demonstrating the scalability of the proposed algorithm.

Fig.3b shows the AQD results over iterations with $(N_T, N_B) = (5, 3)$. Q-functions of all algorithms are initialized to very small random but identical values (thus AQD of all algorithms start at the same value). AQD values for all algorithms decrease over time with varying decay rates, convergence behavior, and convergence points. This result demonstrates that our algorithm converges numerically to the optimal Q-functions, with a convergence rate 25% faster than CTDE and DNA algorithms, and 35% faster fully decentralized algorithms. This result follows from the fast exploration and convergence properties of the single-agent MEMQ and the purely decentralized nature of agents in uncoordinated states. This result also shows the accuracy and convergence of the Bayesian joint state estimation technique. Our algorithm has a similar converge speed to the centralized algorithm, which is consistent with Fig.3a. We also observe that decentralized algorithms (e.g., HQ and I2Q) and deep RL algorithms (e.g., DQN) may not always converge to the optimal Q-functions. We underline that algorithms have similar trends in Fig.3a and Fig.3b (e.g. HQ has the largest AQD as it does not converge, which also leads to a very large APE in the limit).

We finally evaluate the sensitivity of Algorithm 1 by varying several wireless parameters within reasonable ranges and measuring the mean change in APE and AQD. Only one parameter is changed each time, while the others are held constant at the values that minimize APE. The results are summarized in Table IV. We observe that APE and AQD vary at most by 8% and 12%, which indicates a stable performance. The parameters L and Δ_L directly affect the state-space size, but the change in these parameters results in a minimal performance change, showing the efficiency of our algorithm in moderately large discrete state-spaces.

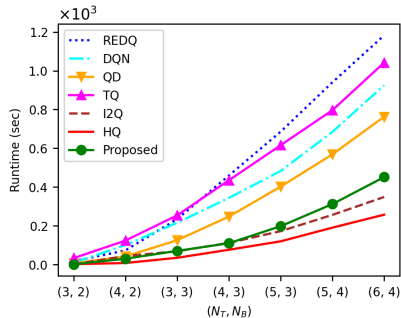


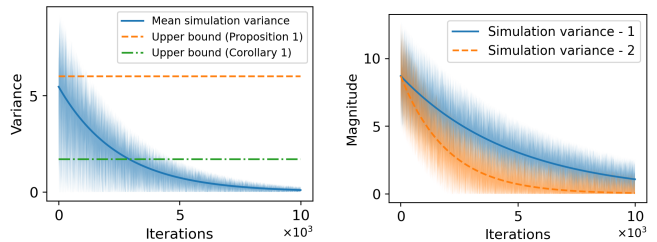
Fig. 4: Runtime of different MARL algorithms

B. Complexity

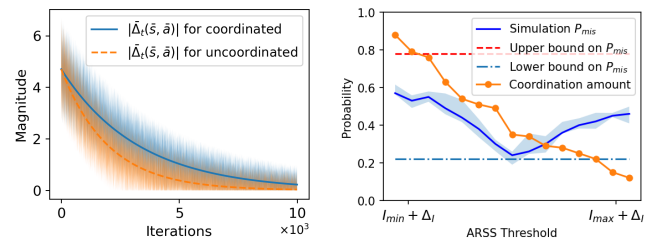
In order to evaluate the complexity of Algorithm 1, we first consider *computational runtime complexity* – the time required for convergence with optimized parameters on the same hardware. Though runtime varies by hardware, we focus on the relative complexity between different algorithms. Some algorithms may not converge to the optimal Q -functions; in such cases, we terminate the algorithm once it converges to a stable point. Fig.4 shows the runtime results across increasing (N_T, N_B) . While all algorithms show an increase in runtime as the wireless network grows, our algorithm has a relatively small increase. In particular, our algorithm can achieve up to 50% less runtime than fully centralized, CTDE and DNA algorithms, particularly across large (N_T, N_B) . This efficiency stems from (i) a fully decentralized approach in uncoordinated states, which eliminates unnecessary coordination and information exchange among agents; (ii) minimal information sharing in coordinated states through only the leader transmitter, which avoids expensive and redundant communication between all agents, and (iii) leveraging fast exploration capabilities of digital cousins and fast convergence of single-agent MEMQ. While decentralized algorithms assume full independence between agents without any coordination or communication, and hence have the smallest runtime, our algorithm has only %10 larger runtime than the decentralized algorithms. We underline that this result is consistent with Fig.3b as plotting the AQD values of algorithms over iterations for different (N_T, N_B) values yields similar plots to Fig.4 (i.e. similar algorithm orders).

One can also consider the *algorithm sample complexity* – the number of training samples (or interactions with the environment) needed to achieve good policies. To this end, we can determine the time index at which the AQD in (22) falls below some threshold. This index is proportional to the sample complexity, as the total number of training samples obtained by iteration t is $t \times l$. Fig. 3b provides an example where our algorithm achieves an AQD of less than 1 in 22000 iterations, while other algorithms need at least 40000 iterations, resulting in a 45% reduction in sample complexity. This improvement becomes greater for smaller thresholds (e.g. 55% reduction in sample complexity to reach AQD < 0.5).

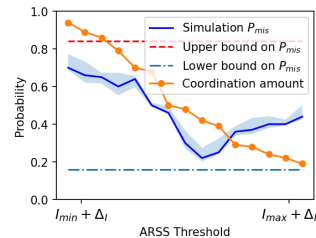
Extensive simulations also show that both the computational runtime and sample complexity of our algorithm are primarily dominated by the slowest agent (i.e. the slowest MEMQ). This is expected, as the joint system cannot converge until all individual systems do. Therefore, optimizing the slowest agent



(a) Simulation variance vs. upper bounds on variance for uncoordinated states (b) Simulation variance vs. upper bounds on variance for coordinated states



(c) Behavior of $\bar{\Delta}_t(\bar{s}, \bar{a})$ (d) Simulation P_{mis} vs. upper and lower bounds on P_{mis} with $N_T = 2$



(e) Simulation P_{mis} vs. upper and lower bounds on P_{mis} with $N_T = 5$

Fig. 5: Numerical validation of theoretical results.

is an effective strategy for enhancing the overall complexity of the joint system.

The memory complexity of Algorithm 1 (i.e., storing local and global Q -functions for each agent), is not explicitly addressed in this paper; however, it can be handled by employing the structural state-aggregation algorithm presented in [8], which is successfully employed for wireless networks in [5].

C. Numerical consistency of propositions

In this section, we simulate the results in the propositions and compare theoretical results with simulation results. The same numerical parameters in Section VI are employed (with $N_T = 3$, $N_B = 2$). We first numerically compute the variance expression in Proposition 1 as in [4]:

$$\mathbb{V}[\mathcal{E}_t(\bar{s}, \bar{a})] \approx \frac{1}{2\Delta_t} \sum_{i=t-\Delta_t}^{t+\Delta_t} \mathcal{E}_i(\bar{s}, \bar{a})^2 - \left[\frac{1}{2\Delta_t} \sum_{i=t-\Delta_t}^{t+\Delta_t} \mathcal{E}_i(\bar{s}, \bar{a}) \right]^2, \quad (23)$$

where $\mathcal{E}_t(\bar{s}, \bar{a}) = \bar{Q}_t(\bar{s}, \bar{a}) - \sum_{i=1}^{N_T} Q_i^*(s_i, a_i)$ with $\Delta_t \ll t$.

The upper bounds on the variance from Proposition 1 and Corollary 1 (with $K_1 = K_2 = K_3 = 2$) and the simulation variance for the **uncoordinated** state-action pair $(\bar{s}, \bar{a}) = (10, 2)$ are shown in Fig.5a. The mean error variance approaches 0 with more iterations. The upper bound from Proposition 1

holds for all t , whereas the upper bound from Corollary 1 holds in the limit (i.e. when the algorithm converges). This result also validates the assumption (10) as both bounds hold. A similar plot for the expectation of $\mathcal{E}(\bar{s}, \bar{a})$ can also be shown, which numerically validates the mean-square convergence of Algorithm 1 in uncoordinated states.

Fig.5b shows two variances for the **coordinated** state-action pair $(\bar{s}, \bar{a}) = (40, 1)$. The orange dotted curve represents the variance of $\bar{Q}_t(\bar{s}, \bar{a}) - \sum_{i=1}^{N_T} Q_i^*(s_i, a_i)$ (which converges to 0) while the blue solid curve shows the variance of $\bar{Q}_t(\bar{s}, \bar{a}) - \bar{Q}^*(\bar{s}, \bar{a})$ (which converges to some non-zero value), and the shaded areas represent the standard deviation over 200 simulations. This result shows that the joint Q -functions of coordinated states converge to $\bar{Q}^*(\bar{s}, \bar{a})$, not to the sum of individual optimal Q -functions $\sum_{i=1}^{N_T} Q_i^*(s_i, a_i)$ as in uncoordinated states, due to coordination between agents, which also shows that $\bar{Q}^*(\bar{s}, \bar{a}) \neq \sum_{i=1}^{N_T} Q_i^*(s_i, a_i)$. Although these two quantities are related, deriving a closed-form relationship is challenging as it depends on real-time ARSS measurements and the ARSS threshold.

Fig.5c shows the evolution of $|\bar{\Delta}_t(\bar{s}, \bar{a})|$ over time for the **coordinated** state-action pair $(\bar{s}, \bar{a}) = (40, 1)$ and **uncoordinated** state-action pair $(\bar{s}, \bar{a}) = (10, 2)$. Clearly, it approaches 0 (with different speeds) for both state-action pairs, which verifies the deterministic convergence of Algorithm 1, and the validity of Proposition 3 (and thus Proposition 2). We underline that while Propositions 2 and 3 are derived for uncoordinated states, the results apply to **both** uncoordinated and coordinated states.

Fig.5d illustrates the simulation misdetection probability (P_{mis}) vs. ARSS threshold I_{thr} , which varies in $[I_{min}, I_{max}]$, along with the upper and lower bounds from Proposition 4 for $N_T = 2$, and the coordination percentage (i.e. $\frac{|S_e|}{|S|}$), where the blue shaded area represents the standard deviation over 200 simulations. We make several observations. First, the upper and lower bounds in Proposition 4 hold for any ARSS threshold value. Second, there is a unique ARSS threshold that minimizes the P_{mis} , which can also be theoretically obtained in Proposition 4. Third, as the ARSS threshold increases, the proportion of coordinated states decreases monotonically. When P_{mis} is minimized, coordinated states make up around 35%, indicating that even in the optimal scenario, the system largely operates independently. Fourth, P_{mis} is larger when I_{thr} is very small (close to the minimum ARSS measurement) than when it is very large (close to the maximum ARSS measurement). This is expected as large I_{thr} causes most states to be uncoordinated, reducing the likelihood of misdetection. Similarly, even though I_{thr} changes significantly, the change in P_{mis} remains relatively modest, demonstrating the robustness of the system to change in system parameters as in Table IV.

Fig.5e presents very similar results for the $N_T = 5$ case along with the bounds from Corollary 2. Similar results also hold for larger N_T . Both bounds hold across all I_{thr} values, but are relatively looser compared to $N_T = 2$ case. The variation in P_{mis} is also larger, indicating that the system is more sensitive to the threshold choice – this is expected as coordination now depends on inputs from multiple agents.

When I_{thr} is very small, most states are coordinated since more agents in close proximity lead to higher ARSS values, which will likely be larger than the ARSS threshold, making the states coordinated. Similar trends can be observed for larger N_T with relatively larger P_{mis} for a given I_{thr} and looser bounds.

VII. CONCLUSIONS

In this paper, we present a novel multi-agent MEMQ algorithm for cooperative decentralized wireless networks with multiple networked transmitters (TXs) and base stations (BSs) to address the performance and complexity limitations of single-agent MEMQ and existing MARL algorithms. Transmitters lack access to global information but can locally measure ARSS due to other TXs. TXs act independently to minimize their individual costs in uncoordinated states. In coordinated states, they employ a Bayesian approach to estimate the joint state based on local ARSS measurements and share limited information with only the leader TX to minimize the joint cost. This communication scheme incurs an information-sharing cost that scales only linearly with the number of TXs, independent of the joint state-action space size. We provide several deterministic and probabilistic theoretical results, including convergence, upper bounds on estimation error variance, and state misdetection probability. We numerically show that our algorithm outperforms several decentralized and CTDE algorithms by achieving 55% lower APE with 50% lower runtime complexity and 35% faster convergence with 45% less sample complexity. It significantly reduces the complexity of centralized algorithms while achieving comparable APE. In the end, it is shown that the simulation results closely follow the theoretical results. For our future work, we work on developing a theoretical sample complexity expression to enable direct comparison with MARL algorithms. We also want to address the continuous state-spaces by combining appropriate deep RL algorithms with our algorithm. Finally, we focus on devising computationally efficient sampling methods to ensure good data coverage across all environments and all agents as in [35], [36].

APPENDIX

A. Proof of Proposition 2

We first rewrite (4) as follows:

$$Q_{i,t}^e = uQ_{i,t}^e + (1-u) \sum_{n=1}^{K_i} w_{i,t}^{(n)} Q_{i,t}^{(n)}, \quad (24)$$

where we drop the (s_i, a_i) notation for simplicity and introduce time subscript t . By repeatedly plugging the expression of $Q_{i,t-1}^e$ into the expression of $Q_{i,t}^e$ in (24), the following can be shown:

$$Q_{i,t}^e = (1-u) \sum_{i=0}^{t-1} u^{t-i-1} \sum_{n=1}^K w_{i,t}^{(n)} Q_{i,t}^{(n)}. \quad (25)$$

Using (25) and algebraic manipulations, we can show:

$$Q_{i,t}^e - uQ_{i,t-1}^e = (1-u) \sum_{n=1}^K w_{i,t-1}^{(n)} Q_{i,t-1}^{(n)}. \quad (26)$$

Let $\Delta_{i,t} = Q_{i,t+1}^e - Q_{i,t}^e$, $\epsilon_{i,t}^{(n)} = w_{i,t+1}^{(n)} Q_{i,t+1}^{(n)} - w_{i,t}^{(n)} Q_{i,t}^{(n)}$. If we rewrite (26) with the variable change $t \rightarrow t+1$, and subtract (26) from the new expression side by side, we obtain:

$$\Delta_{i,t} - u\Delta_{i,t-1}^t = (1-u) \sum_{n=1}^K \left[w_{i,t}^{(n)} Q_{i,t}^{(n)} - w_{i,t-1}^{(n)} Q_{i,t-1}^{(n)} \right]. \quad (27)$$

Then, we can show the following:

$$\Delta_{i,t} = u\Delta_{i,t-1} + (1-u) \sum_{n=1}^K \epsilon_{i,t-1}^{(n)}. \quad (28)$$

$$< \Delta_{i,t-1} + (1-u) \sum_{n=1}^K \epsilon_{i,t-1}^{(n)}, \quad (29)$$

where (28) follows from (27) and the definition of $\epsilon_{i,t-1}^{(n)}$ and (29) follows from the fact that $u \in (0, 1)$. Then, using (29) and the triangle inequality, we can bound the difference between consecutive updates as follows:

$$|\Delta_{i,t} - \Delta_{i,t-1}| < (1-u) \sum_{n=1}^K |\epsilon_{i,t-1}^{(n)}|. \quad (30)$$

Herein, $\lim_{t \rightarrow \infty} Q_{i,t-1}^{(n)} = Q_{i,t}^{(n)}$ by the convergence of Q-learning [34] and $\lim_{t \rightarrow \infty} w_{i,t-1}^{(n)} = w_{i,t}^{(n)}$ by the convergence of the weights [5] for all i, n . Thus, $\lim_{t \rightarrow \infty} |\epsilon_{i,t-1}^{(n)}| = 0$ for all i, n , and hence:

$$\lim_{t \rightarrow \infty} |\Delta_{i,t} - \Delta_{i,t-1}| = 0, \quad \forall i. \quad (31)$$

Using the definition of $\bar{\Delta}_t(\bar{s}, \bar{a})$, we can show:

$$\bar{\Delta}_t(\bar{s}, \bar{a}) = \bar{Q}_t(\bar{s}, \bar{a}) - \bar{Q}_{t-1}(\bar{s}, \bar{a}). \quad (32)$$

$$= \sum_{i=1}^{N_T} (Q_{i,t}^e(s_i, a_i) - Q_{i,t-1}^e(s_i, a_i)). \quad (33)$$

$$= \sum_{i=1}^{N_T} \Delta_{i,t}(s_i, a_i), \quad (34)$$

where (33) follows from the update rule in Table II and (34) follows from the definition of $\Delta_{i,t}$. Then:

$$\begin{aligned} & \lim_{t \rightarrow \infty} |\bar{\Delta}_t(\bar{s}, \bar{a}) - \bar{\Delta}_{t-1}(\bar{s}, \bar{a})| = \\ & = \lim_{t \rightarrow \infty} \left| \sum_{i=1}^{N_T} (\Delta_{i,t}(s_i, a_i) - \Delta_{i,t-1}(s_i, a_i)) \right|, \quad (35) \end{aligned}$$

$$\leq \sum_{i=1}^{N_T} \lim_{t \rightarrow \infty} (\Delta_{i,t}(s_i, a_i) - \Delta_{i,t-1}(s_i, a_i)), \quad (36)$$

$$= 0, \quad (37)$$

where (35) follows from (34), (36) follows from the linearity of expectation and triangle inequality, (37) follows from (31), where we introduce the notation (s_i, a_i) back.

B. Proof of Proposition 4

The probability of detection error is the sum of probabilities for misdetecting a coordinated state as uncoordinated and vice versa. Let \bar{s} be the actual state, and \hat{s} be the detected state.

$$P_{\text{err}} = P(\bar{s} = \text{U}, \hat{s} = \text{C}) + P(\bar{s} = \text{C}, \hat{s} = \text{U}). \quad (38)$$

$$= P(\bar{s} = \text{U} \mid \hat{s} = \text{C})P(\hat{s} = \text{C}) + P(\bar{s} = \text{C} \mid \hat{s} = \text{U})P(\hat{s} = \text{U}). \quad (39)$$

$$= P(I_t < I_{\text{thr}} \mid \hat{s} = \text{C}) \frac{|\mathcal{S}_C|}{|\mathcal{S}|} + P(I_t > I_{\text{thr}} \mid \hat{s} = \text{U}) \frac{|\mathcal{S}_U|}{|\mathcal{S}|}. \quad (40)$$

$$= Q\left(\frac{I_{t,\text{true}} - I_{\text{thr}}}{\sigma_c}\right) \frac{|\mathcal{S}_C|}{|\mathcal{S}|} + Q\left(\frac{I_{\text{thr}} - I_{t,\text{true}}}{\sigma_u}\right) \frac{|\mathcal{S}_U|}{|\mathcal{S}|}, \quad (41)$$

where (38) follows from the definition of misdetection, (39) follows from the Bayes rule, (40) follows from the ARSS criteria used to determine the state, and (41) follows from the noisy ARSS model in (17). We take the gradient of (41) with respect to I_{thr} to find the critical points:

$$\begin{aligned} \frac{dP_{\text{err}}}{dI_{\text{thr}}} &= \frac{1}{\sigma_c} Q' \left(\frac{I_{t,\text{true}} - I_{\text{thr}}}{\sigma_c} \right) \frac{|\mathcal{S}_C|}{|\mathcal{S}|} - \\ & \quad \frac{1}{\sigma_u} Q' \left(\frac{I_{\text{thr}} - I_{t,\text{true}}}{\sigma_u} \right) \frac{|\mathcal{S}_U|}{|\mathcal{S}|}. \quad (42) \end{aligned}$$

$$= -\frac{|\mathcal{S}_C|}{|\mathcal{S}| \sigma_c \sqrt{2\pi}} e^{-\frac{(I_{t,\text{true}} - I_{\text{thr}})^2}{2\sigma_c^2}} + \frac{|\mathcal{S}_U|}{|\mathcal{S}| \sigma_u \sqrt{2\pi}} e^{-\frac{(I_{\text{thr}} - I_{t,\text{true}})^2}{2\sigma_u^2}}. \quad (43)$$

Setting (43) to zero, and taking the natural logarithm on both sides, we obtain:

$$I_{\text{thr}} = I_{t,\text{true}} \pm \sqrt{2 \ln \left(\frac{|\mathcal{S}_C| \sigma_u}{|\mathcal{S}_U| \sigma_c} \right) \left(\frac{1}{\sigma_c^2} - \frac{1}{\sigma_u^2} \right)^{-1}}. \quad (44)$$

If we plug this expression into (41), we obtain:

$$P_{\text{err}} \geq Q\left(\frac{\Delta_I}{\sigma_c}\right) \frac{|\mathcal{S}_C|}{|\mathcal{S}|} + Q\left(\frac{-\Delta_I}{\sigma_u}\right) \frac{|\mathcal{S}_U|}{|\mathcal{S}|}. \quad (45)$$

On the other hand, if $I_{t,\text{true}} - I_{\text{thr}} < 0$, then $\frac{d^2 P_{\text{err}}}{dI_{\text{thr}}^2} < 0$, indicating that (41) is concave in I_{thr} and $I_{\text{thr}} = I_{t,\text{true}} + \Delta_I$ is the global maximum, as $\Delta_I > 0$. If we plug this into (41), we obtain:

$$P_{\text{err}} \leq Q\left(\frac{-\Delta_I}{\sigma_c}\right) \frac{|\mathcal{S}_C|}{|\mathcal{S}|} + Q\left(\frac{\Delta_I}{\sigma_u}\right) \frac{|\mathcal{S}_U|}{|\mathcal{S}|}. \quad (46)$$

REFERENCES

- [1] Wan-Kyu Yun and Sang-Jo Yoo. Q-learning-based data-aggregation-aware energy-efficient routing protocol for wireless sensor networks. *IEEE Access*, 9:10737–10750, 2021.
- [2] Seungmin Lee, Heejung Yu, and Howon Lee. Multiagent q-learning-based multi-uav wireless networks for maximizing energy efficiency: Deployment and power control strategy design. *IEEE Internet of Things Journal*, 9(9):6434–6442, 2021.
- [3] Jesse Clifton and Eric Laber. Q-learning: Theory and applications. *Annual Review of Statistics and Its Application*, 7(1):279–301, 2020.

- [4] Talha Bozkus and Urbashi Mitra. Multi-timescale ensemble q -learning for markov decision process policy optimization. *IEEE Transactions on Signal Processing*, 72:1427–1442, 2024.
- [5] Talha Bozkus and Urbashi Mitra. Leveraging digital cousins for ensemble q -learning in large-scale wireless networks. *IEEE Transactions on Signal Processing*, 72:1114–1129, 2024.
- [6] Talha Bozkus and Urbashi Mitra. A novel ensemble q -learning algorithm for policy optimization in large-scale networks. In *2023 57th Asilomar Conference on Signals, Systems, and Computers*, pages 1381–1386. IEEE, 2023.
- [7] Talha Bozkus and Urbashi Mitra. Ensemble graph q -learning for large scale networks. In *ICASSP 2023 - 2023 IEEE International Conference on Acoustics, Speech and Signal Processing (ICASSP)*, pages 1–5, 2023.
- [8] Talha Bozkus and Urbashi Mitra. Ensemble link learning for large state space multiple access communications. In *2022 30th European Signal Processing Conference (EUSIPCO)*, pages 747–751, 2022.
- [9] Tianxu Li, Kun Zhu, Nguyen Cong Luong, Dusit Niyato, Qihui Wu, Yang Zhang, and Bing Chen. Applications of multi-agent reinforcement learning in future internet: A comprehensive survey. *IEEE Communications Surveys & Tutorials*, 24(2):1240–1279, 2022.
- [10] Amal Feriani and Ekram Hossain. Single and multi-agent deep reinforcement learning for ai-enabled wireless networks: A tutorial. *IEEE Communications Surveys & Tutorials*, 23(2):1226–1252, 2021.
- [11] Yu Bai, Hui Zhao, Xin Zhang, Zheng Chang, Riku Jäntti, and Kun Yang. Toward autonomous multi-uav wireless network: A survey of reinforcement learning-based approaches. *IEEE Communications Surveys & Tutorials*, 25(4):3038–3067, 2023.
- [12] Yu-Jia Chen, Kai-Min Liao, Meng-Lin Ku, Fung Po Tso, and Guan-Yi Chen. Multi-agent reinforcement learning based 3d trajectory design in aerial-terrestrial wireless caching networks. *IEEE Transactions on Vehicular Technology*, 70(8):8201–8215, 2021.
- [13] Ye Hu, Mingzhe Chen, Walid Saad, H Vincent Poor, and Shuguang Cui. Distributed multi-agent meta learning for trajectory design in wireless drone networks. *IEEE Journal on Selected Areas in Communications*, 39(10):3177–3192, 2021.
- [14] Yiding Yu, Soung Chang Liew, and Taotao Wang. Multi-agent deep reinforcement learning multiple access for heterogeneous wireless networks with imperfect channels. *IEEE Transactions on Mobile Computing*, 21(10):3718–3730, 2021.
- [15] Ziyang Guo, Zhenyu Chen, Peng Liu, Jianjun Luo, Xun Yang, and Xinghua Sun. Multi-agent reinforcement learning-based distributed channel access for next generation wireless networks. *IEEE Journal on Selected Areas in Communications*, 40(5):1587–1599, 2022.
- [16] Xinyue Chen, Che Wang, Zijian Zhou, and Keith Ross. Randomized ensembled double q -learning: Learning fast without a model. *arXiv preprint arXiv:2101.05982*, 2021.
- [17] Jayesh K Gupta, Maxim Egorov, and Mykel Kochenderfer. Cooperative multi-agent control using deep reinforcement learning. In *Autonomous Agents and Multiagent Systems: AAMAS 2017 Workshops, Best Papers, São Paulo, Brazil, May 8-12, 2017, Revised Selected Papers 16*, pages 66–83. Springer, 2017.
- [18] Ryan Lowe, Yi I Wu, Aviv Tamar, Jean Harb, OpenAI Pieter Abbeel, and Igor Mordatch. Multi-agent actor-critic for mixed cooperative-competitive environments. *Advances in neural information processing systems*, 30, 2017.
- [19] Soumya Kar, José M. F. Moura, and H. Vincent Poor. QD -learning: A collaborative distributed strategy for multi-agent reinforcement learning through consensus + innovations. *IEEE Transactions on Signal Processing*, 61(7):1848–1862, 2013.
- [20] Francisco S Melo and Manuela Veloso. Learning of coordination: Exploiting sparse interactions in multiagent systems. In *Proceedings of The 8th International Conference on Autonomous Agents and Multiagent Systems-Volume 2*, pages 773–780. Citeseer, 2009.
- [21] Laëtitia Matignon, Guillaume J Laurent, and Nadine Le Fort-Piat. Hysteretic q -learning: an algorithm for decentralized reinforcement learning in cooperative multi-agent teams. In *2007 IEEE/RSJ International Conference on Intelligent Robots and Systems*, pages 64–69. IEEE, 2007.
- [22] Jiechuan Jiang and Zongqing Lu. I2q: A fully decentralized q -learning algorithm. *Advances in Neural Information Processing Systems*, 35:20469–20481, 2022.
- [23] Annie Wong, Thomas Bäck, Anna V Kononova, and Aske Plaat. Deep multiagent reinforcement learning: Challenges and directions. *Artificial Intelligence Review*, 56(6):5023–5056, 2023.
- [24] Changxi Zhu, Mehdi Dastani, and Shihan Wang. A survey of multi-agent deep reinforcement learning with communication. *Autonomous Agents and Multi-Agent Systems*, 38(1):4, 2024.
- [25] Thanh Doan, Siva Maguluri, and Justin Romberg. Finite-time analysis of distributed td (0) with linear function approximation on multi-agent reinforcement learning. In *International Conference on Machine Learning*, pages 1626–1635. PMLR, 2019.
- [26] David Silver, Julian Schrittwieser, Karen Simonyan, Ioannis Antonoglou, Aja Huang, Arthur Guez, Thomas Hubert, Lucas Baker, Matthew Lai, Adrian Bolton, et al. Mastering the game of go without human knowledge. *nature*, 550(7676):354–359, 2017.
- [27] Kaiqing Zhang, Zhuoran Yang, Han Liu, Tong Zhang, and Tamer Başar. Finite-sample analysis for decentralized batch multiagent reinforcement learning with networked agents. *IEEE Transactions on Automatic Control*, 66(12):5925–5940, 2021.
- [28] Chao Yu, Akash Velu, Eugene Vinitzky, Jiaxuan Gao, Yu Wang, Alexandre Bayen, and Yi Wu. The surprising effectiveness of ppo in cooperative multi-agent games. *Advances in Neural Information Processing Systems*, 35:24611–24624, 2022.
- [29] Justin K Terry, Nathaniel Grammel, Sanghyun Son, and Benjamin Black. Parameter sharing for heterogeneous agents in multi-agent reinforcement learning. *arXiv e-prints*, pages arXiv–2005, 2020.
- [30] Zepeng Ning and Lihua Xie. A survey on multi-agent reinforcement learning and its application. *Journal of Automation and Intelligence*, 2024.
- [31] Geng Sun, Wenwen Xie, Dusit Niyato, Fang Mei, Jiawen Kang, Hongyang Du, and Shiwen Mao. Generative ai for deep reinforcement learning: Framework, analysis, and use cases. *IEEE Wireless Communications*, 2025.
- [32] Vincent Huang, Tobias Ley, Martha Vlachou-Konchylaki, and Wenfeng Hu. Enhanced experience replay generation for efficient reinforcement learning. *arXiv preprint arXiv:1705.08245*, 2017.
- [33] Thang Doan, Bogdan Mazouze, and Clare Lyle. Gan q -learning. *arXiv preprint arXiv:1805.04874*, 2018.
- [34] Francisco S Melo. Convergence of q -learning: A simple proof. *Institute Of Systems and Robotics, Tech. Rep.*, pages 1–4, 2001.
- [35] Talha Bozkus and Urbashi Mitra. Coverage analysis of multi-environment q -learning algorithms for wireless network optimization. In *2024 IEEE 25th International Workshop on Signal Processing Advances in Wireless Communications (SPAWC)*, pages 376–380. IEEE, 2024.
- [36] Talha Bozkus, Tara Javidi, and Urbashi Mitra. Coverage analysis for digital cousin selection—improving multi-environment q -learning. *arXiv preprint arXiv:2411.08360*, 2024.
- [37] Louie Chan, Karina Gomez Chavez, Heiko Rudolph, and Akram Hourani. Hierarchical routing protocols for wireless sensor network: A compressive survey. *Wireless Networks*, 26:3291–3314, 2020.
- [38] Zheng Yang, Zimu Zhou, and Yunhao Liu. From rssi to csi: Indoor localization via channel response. *ACM Computing Surveys (CSUR)*, 46(2):1–32, 2013.
- [39] Yuanyuan Wu, Haipeng Chen, and Feng Zhu. Dcl-aim: Decentralized coordination learning of autonomous intersection management for connected and automated vehicles. *Transportation Research Part C: Emerging Technologies*, 103:246–260, 2019.
- [40] Chao Yu, Minjie Zhang, Fenghui Ren, and Guozhen Tan. Multiagent learning of coordination in loosely coupled multiagent systems. *IEEE Transactions on Cybernetics*, 45(12):2853–2867, 2015.
- [41] Yu-Jia Chen, Deng-Kai Chang, and Cheng Zhang. Autonomous tracking using a swarm of uavs: A constrained multi-agent reinforcement learning approach. *IEEE Transactions on Vehicular Technology*, 69(11):13702–13717, 2020.
- [42] Talha Bozkus and Urbashi Mitra. Link analysis for solving multiple-access mdps with large state spaces. *IEEE Transactions on Signal Processing*, 71:947–962, 2023.
- [43] Talha Bozkus and Urbashi Mitra. A multi-agent multi-environment mixed q -learning for partially decentralized wireless network optimization. *arXiv preprint arXiv:2409.16450*, 2024.
- [44] Sebastian Thrun and Anton Schwartz. Issues in using function approximation for reinforcement learning. In *Proceedings of the 1993 Connectionist Models Summer School Hillsdale, NJ. Lawrence Erlbaum*, volume 6, pages 1–9, 1993.
- [45] Talha Bozkus and Urbashi Mitra. Appendix. <https://github.com/talhabozkus/MARL-supplementary-appendix>, 2025.